Developmental Biology 353 (2011) 81–93

Contents lists available at ScienceDirect

Developmental Biology

journal homepage: www.elsevier.com/developmentalbiology

P58-A and P58-B: Novel proteins that mediate skeletogenesis in the sea urchin embryo

Ashrifia Adomako-Ankomah, Charles A. Ettensohn *

Department of Biological Sciences, Carnegie Mellon University, 4400 Fifth Avenue, Pittsburgh, PA 15213, USA

ARTICLE INFO

Article history:
Received for publication 27 January 2011
Revised 17 February 2011
Accepted 18 February 2011
Available online 26 February 2011

Keywords:
Sea urchin embryo
P58
Primary mesenchyme cells
Skeletogenesis
Morphogenesis
Biomineralization
Gene regulatory network

ABSTRACT

During sea urchin embryogenesis, the skeleton is produced by primary mesenchyme cells (PMCs). PMCs undergo a sequence of morphogenetic behaviors that includes ingression, directed migration, and cell–cell fusion. Ultimately, PMCs deposit the calcite-containing biomineral that forms the endoskeleton of the late embryo and early larva. The endoskeleton has a stereotypical structure and is the major determinant of the distinctive, angular shape of the larva. Although many candidate biomineralization proteins have been identified, functional data concerning these proteins are scant. Here, we identify and characterize two new biomineralization genes, *p58-a* and *p58-b*. We show that these two genes are highly conserved in *Strongylocentrotus purpuratus* and *Lytechinus variegatus*, two sea urchin species whose ancestors diverged approximately 100 mya. The *p58-a* and *p58-b* genes lie in tandem on the chromosome, suggesting that one of the two genes arose via a gene duplication event. The two genes encode closely related, type I transmembrane proteins. We have established by whole mount in situ hybridization that *p58-a* and *p58-b* are expressed specifically in the PMCs in both species. Knockdown of either gene by morpholino antisense oligonucleotides leads to profound defects in skeletogenesis, although skeletal elements are not completely eliminated. The P58-A and P58-B proteins do not appear to play a role in the specification, directed migration or differentiation of the PMCs, but most likely are directly involved in biomineralization during sea urchin embryonic development.

Introduction

A central objective of developmental biology is to understand how morphology is encoded in the genome. The development of the endoskeleton of the sea urchin embryo provides a valuable experimental model for the genomic encoding of a complex anatomical structure (reviewed by Okazaki, 1975; Wilt and Ettensohn, 2007). The embryonic skeleton is secreted by primary mesenchyme cells (PMCs). PMCs are the progeny of the large micromeres, four cells that arise from unequal cleavage divisions at the vegetal pole of the embryo. At the late blastula stage, PMCs undergo an epithelial-to-mesenchymal transition (EMT) and ingress into the blastocoel (Wu et al., 2007). After ingression, PMCs migrate directionally along the blastocoel wall and adopt a characteristic ring-like pattern (the subequatorial PMC ring). Within the subequatorial ring, clusters of PMCs (the ventrolateral clusters, or VLCs) form at two positions. PMCs begin to fuse with one another soon after EMT, and by the end of gastrulation these cells are joined in a single, common syncytium (Hodor and Ettensohn, 1998). PMC migration and fusion are mediated by numerous, dynamic filopodial protrusions (Gustafson and Wolpert, 1961; Malinda et al., 1995; Miller et al., 1995). Skeletogenesis begins with the deposition of one triradiate spicule rudiment in each VLC. The two spicule rudiments subsequently elongate and branch in a highly stereotypical pattern, thereby producing the complex endoskeleton of the embryo (Gustafson and Wolpert, 1961; Ettensohn and Malinda, 1993). The final structure of the larval endoskeleton is both species-specific and highly reproducible within a species.

Recent studies have begun to elucidate an elaborate gene regulatory network (GRN) that is deployed in the large micromere–PMC lineage (Oliveri et al., 2008; Ettensohn, 2009). The current model of the skeletogenic GRN contains approximately 80 genes. The network is activated by various maternal inputs, including β-catenin, which collectively trigger the expression of several early zygotic regulatory genes, such as *pmar1* (Oliveri et al., 2002), *alx1* (Ettensohn et al., 2003), *ets1* (Kurokawa et al., 1999), and *t-brain* (Croce et al., 2001; Fuchikami et al., 2002), selectively in the micromere–PMC lineage. The transcription factors encoded by these genes provide inputs into other regulatory genes, and various feedback and feedforward interactions among these genes stabilize the transcriptional network and drive it forward (Oliveri et al., 2008).

To understand the genomic wiring of skeletal anatomy it will be essential to identify linkages between regulatory genes and downstream target genes that directly affect skeletal morphology. Recent studies have begun to identify some of the proteins that control

* Corresponding author. Fax: +1 412 268 7129.
E-mail address: ettensohn@andrew.cmu.edu (C.A. Ettensohn).

0012-1606/$ – see front matter © 2011 Elsevier Inc. All rights reserved.
doi:10.1016/j.ydbio.2011.02.021

skeletal morphogenesis. Two receptor tyrosine kinases, VEGFR-Ig-10 and FGFR-2, mediate PMC migration and differentiation (Duloquin et al., 2007; Röttinger et al., 2008). Many candidate biomineralization-related proteins have been identified by a wide variety of methods, including cDNA library screens (Benson et al., 1987; George et al., 1991; Harkey et al., 1995; Lee et al., 1999), genome-wide bioinformatics approaches (Zhu et al., 2001; Illies et al., 2002; Livingston et al., 2006), and proteomics (Mann et al., 2008; Mann et al., 2010a,b). Functional studies on these candidate biomineralization proteins, however, are surprisingly scant. Knockdown of *Strongylocentrotus purpuratus* SM50 (or its *Lytechinus pictus* homolog LSM34) by means of antisense oligonucleotides has shown that this protein is required for biomineralization (Peled-Kamar et al., 2002; Wilt et al., 2008b). Morpholino antisense oligonucleotides have been used to interfere with the expression of P16, a novel, PMC-specific transmembrane protein, and these studies have shown that P16 is essential for skeletal rod elongation, but not for PMC specification, migration, or fusion (Cheers and Ettensohn, 2005).

In this study, we have identified two novel proteins, P58-A and P58-B, that are essential for skeletogenesis. The genes that encode these proteins lie adjacent to one another on the same chromosome and are likely to be the product of a relatively recent gene duplication event. They are expressed specifically in the PMCs of *S. purpuratus* and *Lytechinus variegatus* embryos, and knockdown of either P58-A or P58-B using translation- or splice-blocking morpholinos results in a suppression of skeletogenesis. We have discovered that P58-A and P58-B do not play a role in PMC specification, migration, or fusion, but instead are most likely directly involved in depositing the calcite-based biomineral that composes the sea urchin endoskeleton. The discovery of these genes broadens our knowledge of the genes that interact to form the complex endoskeleton of the sea urchin embryo.

Materials and methods

Embryo culture

Adult *S. purpuratus* were obtained from Pat Leahy (California Institute of Technology, Pasadena, CA). Adult *Lytechinus variegatus* were obtained from Elizabeth Leaser (Wilmington, NC) or from Reeftopia, Inc. (Key West, FL). Spawning was induced by intracoelomic injection of 0.5 M KCl and embryos were cultured in artificial seawater (ASW) at 15 °C (*S. purpuratus*) or at 23 °C (*L. variegatus*).

Gene sequence analysis

The sequences of *S. purpuratus* P58-A and P58-B (designated Sp-P58-A and Sp-P58-B, respectively) were assembled from expressed sequence tags (ESTs) that were obtained as part of a PMC transcriptome project (Zhu et al., 2001; Illies et al., 2002; Livingston et al., 2006). Part of the sequence of *L. variegatus* P58-A (Lv-P58-A) was obtained by screening a *L. variegatus* midgastrula cDNA library (the gift of Dr. David McClay, Duke University). Clone 38-G5 contained all but the 5′-most coding sequence of the mRNA. The remainder of the sequence was obtained by 5′ RACE using the GeneRacer® Kit with SuperScript® III RT and the TOPO TA Cloning® Kit for Sequencing (Invitrogen). The sequence of *L. variegatus* P58-B (Lv-P58-B) was assembled from several *L. variegatus* ESTs kindly provided by Dr. Cynthia Bradham (Boston University) and Dr. Albert Poustka (Max-Planck Institut). Comparisons of the sequences of P58-A and P58-B from *S. purpuratus* and *L. variegatus* were carried out using ClustalW (Thompson et al., 1994). Predicted signal peptide and transmembrane sequences were identified using the SignalP3.0 (Emanuelsson et al., 2007) and DAS transmembrane prediction (Cserzö et al., 1997) programs, respectively.

Whole mount in situ hybridization (WMISH)

Embryos were fixed for 1 h at room temperature in 4% paraformaldehyde in ASW and stored at 4 °C in 100% methanol. WMISH was carried out as described elsewhere (Lepage et al., 1992, Duloquin et al., 2007). *Sp-p58-a* and *Sp-p58-b* probes were synthesized using clones 146-J23 and 151-N12, respectively, from the *S. purpuratus* PMC library as templates. *Lv-p58-a* probe was synthesized using clone 38-G5 from the *L. variegatus* midgastrula library as a template. *Lv-p58-b* probe was synthesized using a 3′ fragment of sequence obtained from initial attempts to clone the gene using the GeneRacer® Kit with SuperScript® III RT and the TOPO TA Cloning® Kit for Sequencing (Invitrogen) as a template. Gene sequence obtained was cloned into the pCR4Blunt TOPO vector. *Lv-p58-b* WMISH was also conducted by cross-hybridization with the *Sp-p58-b* probe. The probe for *Sp-p19* (GLEAN3_04136) was synthesized using clone 13-P18 from the *S. purpuratus* PMC library as a template.

Microinjection of morpholino antisense oligonucleotides (MOs)

Microinjections were carried out following the protocol of Cheers and Ettensohn (2004). Injection solutions contained 20% (vol/vol) glycerol and 0.16% (wt/vol) Texas Red dextran. *Sp-p58-a* splice-blocking MO was complementary to the exon 3/intron 3 boundary (sequence: 5′-ATTCATCATGTTTCGAACTTACGCG-3′). *Sp-p58-b* splice-blocking MO was complementary to the exon 2/intron 2 boundary (sequence: 5′- ACGGCTTCCATCACTAACCTGATTG -3′). *Lv-p58-a* and *Lv-p58-b* translation-blocking MOs were designed to overlap the start codon or 5′-UTR of each mRNA (sequences: 5′-CGTGAGATAAAATA-CACCTTCCATC-3′ and 5′-CTCCTCTTTCCACGATAACAACTGA-3′ respectively). MOs were injected at the following working concentrations: *Sp-p58-a*: 4 mM, *Sp-p58-b*: 2 mM, *Lv-p58-a*: 0.5 mM, *Lv-p58-b*: 0.1 mM.

RT-PCR analysis

For each experiment, RNA was extracted from 200 control and 200 MO-injected *S. purpuratus* embryos using the Nucleospin RNA II kit (Clonetech). cDNA was synthesized using the Ambion Retroscript kit, and PCR was carried out using Platinum Taq High Fidelity DNA Polymerase (Invitrogen). Forward and reverse primers for *Sp-p58-a* were 5′-CACGATCGATCGACCGGTAAGGAGTT-3′ and 5′-GAACTCTA-GACGCTGGGTAACCAAAG-3′, respectively. Forward and reverse primers for *Sp-p58-b* were 5′-CATGCTGGAGAGTTCATTGGGTTCGC-3′ and 5′-GCACTCTAGACTGTCATTGGGTCCGT-3′, respectively. PCR products were analyzed on 1% agarose gels that contained 0.5% ethidium bromide. Bands were gel-purified using the QIAquick® gel extraction kit (Qiagen), and cloned into the pCS2+ vector for sequencing, using the Cla1 and Xba1 restriction sites.

Immunofluorescence

Immunofluorescence using the 6a9 monoclonal antibody was carried out as described previously (Ettensohn and McClay, 1988). Immunostained embryos were examined using a Zeiss LSM 510 Meta/UV DuoScan Inverted Spectral Confocal Microscope.

Fig. 1. Analysis of *p58-a* and *p58-b* gene organization in *S. purpuratus* and comparisons of the predicted amino acid sequences of the P58-A and P58-B proteins in *S. purpuratus* and *L. variegatus*. (A) Schematic of the exon–intron structures of *Sp-p58-a* and *Sp-p58-b* and their locations on Contig NW_001334655.1. (B) ClustalW alignment of the amino acid sequences of P58-A from *S. purpuratus* and *L. variegatus*. (C) ClustalW alignment of the amino acid sequences of P58-B from *S. purpuratus* and *L. variegatus*. (D) ClustalW alignment of amino acid sequences of P58-A and P58-B from *S. purpuratus*. Signal sequences are shown in red, and transmembrane sequences are shown in blue and underlined. Asterisks indicate identical amino acids, and dashes indicate conserved amino acids.

A) Schematic of P58-A and P58-B location on Contig NW_001334655.1.

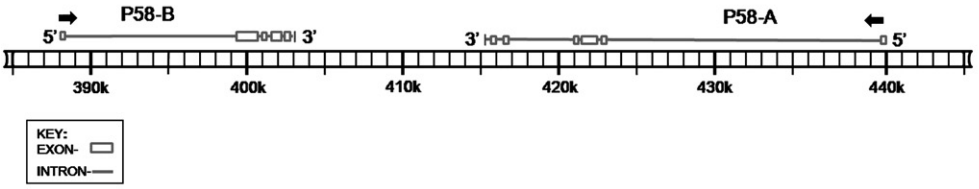

B

```
Sp P58-A    1 MGVIFYLYIALTAMLATLSQAQRAQ---APLDTTGKEFVFAFQSNFQNKR  47
Lv P58-A    1 MEGVFYLYIVLCAMLTTLSQAQPARPGPAPLDTTGKEFVFAFQSNFQNKR  50
              *  .***** *.***.****** *.   **********************

Sp P58-A   48 PDKLSLLIGANEPGLTRVQIEAPNFNWQQTVQLQHKQVRNVDINPDVAAR  97
Lv P58-A   51 PDRLTLLLGANEPGLTRVQVEAPNFNWQQTVQLQHKQVRQVDLNFPDIAAR 100
              **.*.**.**********.******************.**.***.***

Sp P58-A   98 GAGPVNGTLIVRATKDVSISGLNSLTMTNDAFLAIPTHGLGQEYYVASYD 147
Lv P58-A  101 GAGPVNGTLIVRATKDISVHGLNSLTMTNDAFLAIPTHGLGEAYFVASYD 150
              ****************.*. ********************. *.*****

Sp P58-A  148 PVPIEMSQFLITGIQPDTSVKIVLQARLQHNSQWYSKGQTLTVNVGKYQS 197
Lv P58-A  151 PVPIEMSQFLITGIQPDTTVKIVLQARLQHNSQWYSKGQTLTVNVGKYQS 200
              ******************.**************************.*****

Sp P58-A  198 IQFQSQEDLTGTKITSTKPLSVMSGASCTLVPTQVYRCDHLVEHLPPFNT 247
Lv P58-A  201 IQFQSQEDLTGTRITSTKPISVMSGASCTLVPTQVYRCDHLVEHLPPFNT 250
              ************.*******.**************************.***

Sp P58-A  248 WGKRFTLLPFSNRSGGFIFRIIAGRPSTTVHIMGNNVQLQFEGSFREFNQ 297
Lv P58-A  251 WGKRFTLLPFSNRSGGFIFRIIAGRPSTTVHIMGNNVQLQFEGSFREFNQ 300
              **************************************************

Sp P58-A  298 PASLKTTLQSDKPIMVVQYAKGMQKDNNGDPFMTLIPPVEQYMEKEITFG 347
Lv P58-A  301 PASLKTTLQSDKPIMVVQYAKGMQKDNNGDPFMTLIPPVEQYMQKEITFG 350
              **************************************************.******

Sp P58-A  348 SFNQSGTDMLNMFAGVSFTSPALFTMSLNGKPAFEPSTGIPGTGISRTFT 397
Lv P58-A  351 SFNQSGTDMLNMFAGVSFTSPALFTMSLNGKSSFEPDQGIPGTGISSTFT 400
              ********************************.***  ******** ***

Sp P58-A  398 ADATVPLDDVRNILTNYEKDVRFMAVIYGFASGTSFGYPAAYQLRQLTCT 447
Lv P58-A  401 ADSTIPLDNIRNILTNYEKDVHYMAIVYGFASGTSFGYPAAYQLRQITCT 450
              **.*.*** .**********..**..*****************.***

Sp P58-A  448 RPGRQGPEAEYDCPETHRRPRPTAPVVPVGPGGGGDGAAMTGCTSKGVVV 497
Lv P58-A  451 RPGRQGPEAEFECPDSHRRPRPTAPVVPVGPGGGGE-LGGEGCTSKGVVV 499
              **********..**..********************.     **********

Sp P58-A  498 LAAILPALIVFIDMVILLVFVLYRMR-----RKF                 526
Lv P58-A  500 LAAILPALIVFIDMVILLVFVLYRTPSTPELQKFKMFFRVNPRERTISRC 549
              ************************      .**

Sp P58-A  527         526
Lv P58-A  550 SFVRNGSL 557
```

C

```
Sp P58-B    1 MSNLLVLAAVLLQFIGFATPQQAPYLPSNSPTFTVGSPDTRGTKFMFAMP  50
Lv P58-B    1 MSNLLVLSAVLLQYIGYATPQQAPYLPANAPTFNLGSPDTRGTKFMFAIP  50
              *******.*****.**.**********.*.***..*************.*

Sp P58-B   51 SNFNVASKVTLMIGSSNPGIARVMVNIPGFKFRREITLTQRQMKTISIPG 100
Lv P58-B   51 SNFNIPSKVTLMIGSSNPGIARVMVNIPGFKFRREITLTQRQMKTISIPG 100
              ****. **************************************************

Sp P58-B  101 NVAANGGGPQNGTIVVTSNLEITVHAANIMPKTNDAFVAIPTDALGKEYV 150
Lv P58-B  101 NVAANGGGPQNGTIVVTSNLEITVHAANIMPKTNDGFVAIPTDAVGKEYV 150
              ********************************** ********.*****

Sp P58-B  151 IASYDIVTGQWSVFTITGTQQGTRIQVVPSQRTLHARQWYNPGQIINIQL 200
Lv P58-B  151 IASYDIVTGQWSVFTITGTQQGTRIQVVPSQRILHARQWYNAGQIINVQL 200
              ********************************** ******** *****.**

Sp P58-B  201 NEAQSIQIRAPMDLTGTYITADKPVAVVSGATCTRVPKDMQRCDHLVEML 250
Lv P58-B  201 SEAQSVQFRCPDDLTGTYITADKPVAVVSGATCTRVPRSMQRCDHLVEML 250
               ****.* *.* ************************. ***********

Sp P58-B  251 PPISALGTRFSIVPLLNRTGYVFRMIAARPNTRVHMAGVIYTLGQRGSFR 300
Lv P58-B  251 PPISTLGTRFSVLPLLNRTGYVFRMIAARPNTKVHLAGTIYTLGQRGSFR 300
              ****.******..*********************.**.** ***********

Sp P58-B  301 EFNQDAQLPVTITSNRPLLVMQYGKGMDIDFWGDPFMSIVPPVEQYMEGM 350
Lv P58-B  301 EFNQDAQLPVTITSNRPLLVMQYGKGMDVNFWGDPFMSIVPPVEQYMEGM 350
              ****************************. ********************

Sp P58-B  351 TTFGPLAQSGQDRFFSFLSVSVTSADLYTISLDNVLIMNTELNLPLGSET 400
Lv P58-B  351 TTFGPLAQSGQDMFFNFLSVSVTSAYLYTISLNNVLIMNTELNLPEMEET 400
              ************ ** ********* ****** ************   **

Sp P58-B  401 IRYTADRNMRIQNIPHTLHNPSLMSRFTAICHGVSQGSGYGYPIGYNLRT 450
Lv P58-B  401 IRYTADRNMKIQNVPHTLHNPSVMSRFTAICHGVSQGSGYGYPIGYNLRT 450
              *********.***.********.*************************

Sp P58-B  451 LLCSRTDPMTGLIEEFQCPPPIPPIVPGLVPSNVPGMGGNQPIRPGLGMG 500
Lv P58-B  451 LLCSRTDPMTGLIEEFQCPPPIPPIQPGLIPSTVPGMGGNQPIRPGVGMN 500
              ************************ ***.**.************.**.

Sp P58-B  501 -GMGGYGGGYGGMYPGFTTGGQPGGYLPGNFFTGGKALNPNIPILPGLPI 549
Lv P58-B  501 PGMGGFGVGMG-MFPGFSAGGQPGAFLPGNFFTGGKALPFNIPIIPGLPI 549
               ****.* * * *.***..***** .************ *****.*****

Sp P58-B  550 DPNAGAAQTQPGFNNNPLNPVSPNNPFANPGQPFVPMLPFNPMGPGMIPP 599
Lv P58-B  550 DPNAGAAQTQPGFNNNPLNPVSPNNPFANPGQPFVPMLPFNPMGPGMIPP 599
              **************************************************

Sp P58-B  600 PENCYTLGLLILAAVAPVTVVFIVMLVILLAIVYRFKRKN 639
Lv P58-B  600 PENCYTLGLLILAAVAPVTVVFIVMLVILLAIVYRFKRKH 639
              ************************************.
```

D

```
Sp P58-A    1 MGVIFYLYIALTAMLATLSQAQRAQAP----------LDTTGKEFVFAFQ  40
Sp P58-B    1 MSNLLVLAAVLLQFIGFATPQQAPYLPSNSPTFTVGSPDTRGTKFMFAMP  50
              *  .  *.  *   .  .  *   *           ** *  *.**

Sp P58-A   41 SNFQNKRPDKLSLLIGANEPGLTRVQIEAPNFNWQQTVQLQHKQVRNVDI  90
Sp P58-B   51 SNFN---VASKVTLMIGSSNPGIARVMVNIPGFKFRREITLTQRQMKTISI  98
              ***.     *..*.**.  **..** .  *.*  .. . * ..*.... *

Sp P58-A   91 NPDVAARGAGPVNGTLIVRATKDVSISGLNSLTMTNDAFLAIPTHGLGQE 140
Sp P58-B   99 PGNVAANGGGPQNGTIVVTSNLEITVHAANIMPKTNDAFVAIPTDALGKE 148
                 *** * ** ***..* .. ....   * .  *****.****  **.*

Sp P58-A  141 YYVASYDPVPIEMSQFLITGIQPDTSVKIVLQARLQHNSQWYSKGQTLTV 190
Sp P58-B  149 YVIASYDIVTGQWSVFTITGTQQGTRIQVVPSQRTLHARQWYNPGQIINI 198
              * .**** *  . * * *** *  * ...*   *  *  ***  ** ...

Sp P58-A  191 NVGKYQSIQFQSQEDLTGTKITSTKPLSVMSGASCTLVPTQVYRCDHLVE 240
Sp P58-B  199 QLNEAQSIQIRAPMDLTGTYITADKPVAVVSGATCTRVPKDMQRCDHLVE 248
              ...  **** ..  ***** **. **..*.***.** **   . *******

Sp P58-A  241 HLPPFNTWGKRFTLLPFSNRSGGFIFRIIAGRPSTTVHIMGNNVQLQFEG 290
Sp P58-B  249 MLPPISALGTRFSIVPLLNRTG-YVFRMIAARPNTRVHMAGVIYTLGQRG 297
               ***  . * **...*  **.* ..**.** ** * **. *    *  *

Sp P58-A  291 SFREFNQPASLKTTLQSDKPIMVVQYAKGMQKDNNGDPFMTLIPPVEQYM 340
Sp P58-B  298 SFREFNQDAQLPVTITSNRPLLVMQYGKGMDIDFWGDPFMSIVPPVEQYM 347
              ******* * *  *. * .*..*.** ***  *  *****...*******

Sp P58-A  341 EKEITFGSFNQSGTDMLNMFAGVSFTSPALFTMSLNGKPAFEPSTGIPGT 390
Sp P58-B  348 EGMTTFGPLAQSGQDRFFSFLSVSVTSADLYTISLDNVLIMNTELNLPLG 397
              *   ***   *** *     *  ** **  *.*.** .         ..*

Sp P58-A  391 GISRTFTADATVPLDDVRNILTNYEKDVRFMAVIYGFASGTSFGYPAAYQ 440
Sp P58-B  398 SETIRYTADRNMRIQNIPHTLHNPSLMSRFTAICHGVSQGSGYGYPIGYN 447
                .  .*** .. .  . . * *     ** *.  * . *. .***  *.

Sp P58-A  441 LRQLTCTR----------------------------PGRQG--------- 453
Sp P58-B  448 LRTLLCSRTDPMTGLIEEFQCPPPIPPIVPGLVPSNVPGMGGNQPIRPGL 497
              ** * *.*                           **  *

Sp P58-A  454 ------------------------P------------------------- 454
Sp P58-B  498 GMGGMGGYGGGYGGMYPGFTTGGQPGGYLPGNFFTGGKALNPNIPILPGL 547
                                     *

Sp P58-A  455 ------------EAEYDCPETHRRP---------RPTAPVVPVGPGGGGDG 484
Sp P58-B  548 PIDPNAGAAQTQPGFNNNPLNPVSPNNPFANPGQPFVPMLPFNPMGPGMI 597
                           * .  *        .*  *..* .* * *

Sp P58-A  485 AAMTGCTSKGVVVLAAILPALIVFIDMVILLVFVLYRMRRKF 526
Sp P58-B  598 PPPENCYTLGLLILAAVAPVTVVFIVMLVILLAIVYRFKRKN 639
                 .* . *...***. *  .***.*..**. ..** .**
```

PMC fusion assay

PMC fusion was monitored by dye transfer, as described previously (Hodor and Ettensohn, 2008). Briefly, one set of *L. variegatus* fertilized eggs was injected with *Lv-p58-a* MO that contained 10% (wt/vol) fluorescein dextran, while another set of fertilized eggs was injected with *Lv-p58-a* MO that lacked the dextran. At the mesenchyme blastula stage, a few (2–6) PMCs were transferred from a dextran-labeled embryo into an unlabeled host embryo. After 24 h, embryos were visualized with a Zeiss LSM 510 Meta/UV DuoScan Inverted Spectral Confocal Microscope to assess the distribution of the dextran within the PMC syncytium. The same procedure was used to test the role of *Lv-p58-b* in PMC fusion.

Results

p58-A and p58-B encode related, novel proteins and are probably duplicated genes

Sp-P58-A and Sp-P58-B were identified from ESTs that were obtained as part of a PMC transcriptome project (Zhu et al., 2001; Livingston et al., 2006). Upon mapping *Sp-p58-a* and *Sp-p58-b* to contig NW_001334655.1, which was assembled as part of the sea urchin genome project, we observed that these two genes (*GLEAN3_00439* and *GLEAN3_00438*, respectively) lie directly adjacent to one another (Fig. 1A), though they are transcribed in opposite directions. *Sp-p58-a* contains 7 exons and encodes a 526 amino acid protein, and *Sp-p58-b* contains 6 exons and encodes a 639 amino acid protein. We identified a predicted signal sequence at the N-terminus of each protein, and each protein contains a single, predicted transmembrane domain near its C-terminus. Both proteins are basic and are relatively rich in proline, glycine, and threonine residues (Tekaia and Yeramian, 2006). We cloned orthologs of P58-A and P58-B from *L. variegatus*, a species that diverged from *S. purpuratus* approximately 100 mya (Smith et al., 2006). Lv-P58-A and Lv-P58-B are very similar to their *S. purpuratus* orthologs; ClustalW alignments showed that Sp-P58-A and Lv-P58-A are 81% identical (Fig. 1B), and Sp-P58-B and Lv-P58-B are 91% identical (Fig. 1C). Comparisons between P58-A and P58-B within each species showed that the two paralogs are less well conserved than the orthologous pairs; the former are approximately 34% identical and 16% similar in both species (Fig. 1D and data not shown).

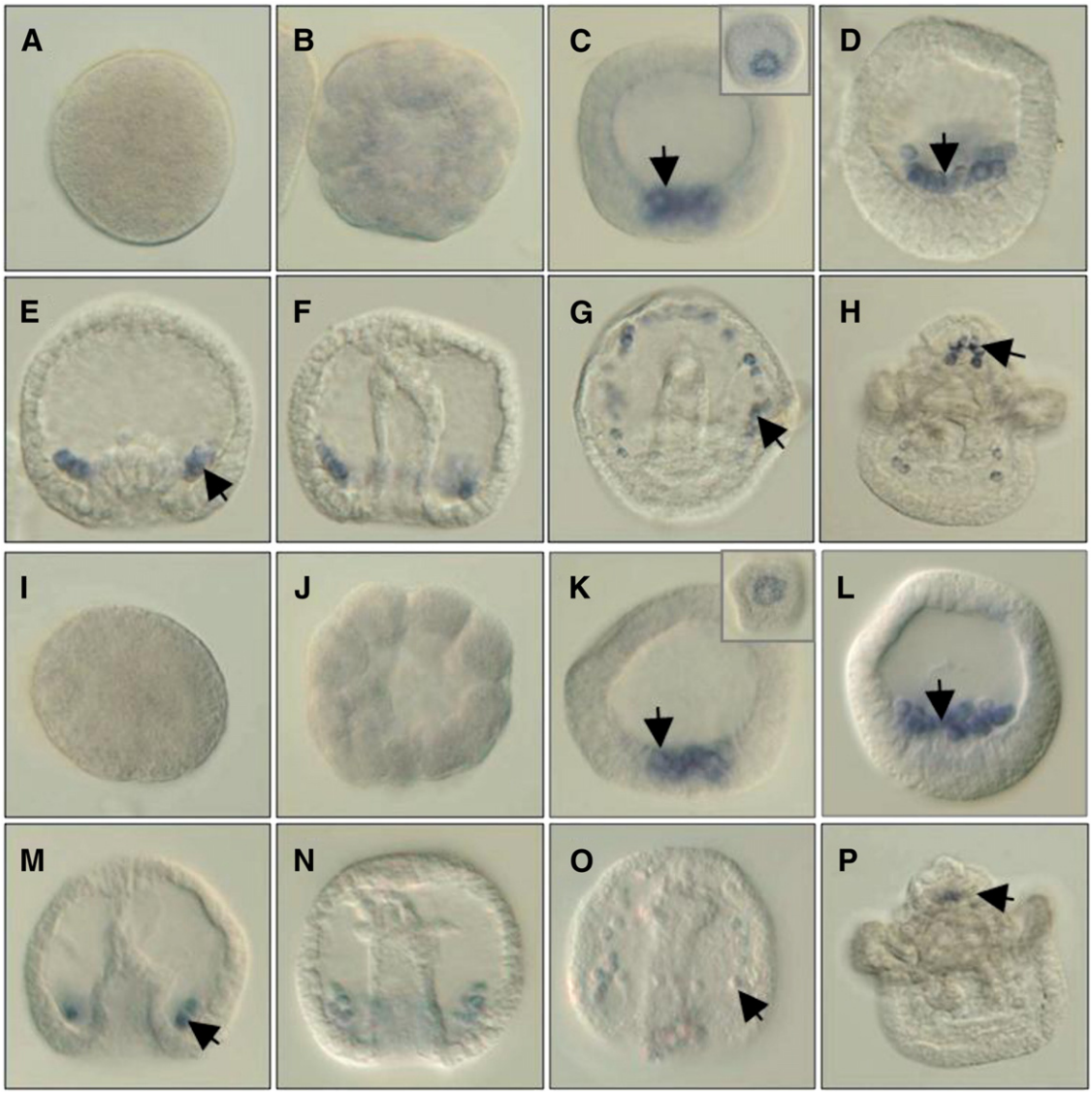

Fig. 2. Whole mount in situ hybridization analysis of *p58-a* (A–H) and *p58-b* (I–P) expression in *S. purpuratus*. Expression of *p58-a* is undetectable prior to hatching (A and B). Staining is visible after hatching and is restricted to PMCs throughout later development (arrows, C–H). Expression of *p58-b* is also undetectable prior to hatching (I and J), but is apparent in PMCs from hatching until at least the late gastrula stage (arrows, K–N), after which time expression is significantly reduced (O and P). (A and I) Unfertilized egg. (B and J) Cleavage stage. (C and K) Hatched blastula. (D and L) Mesenchyme blastula. (E and M) Early gastrula. (F and N) Late gastrula. (G and O) Prism. (H and P) Pluteus larva.

p58-a and p58-b mRNAs are restricted to PMCs

We analyzed the patterns of expression of *p58-a* and *p58-b* in *S. purpuratus* (Fig. 2) and *L. variegatus* (Fig. 3) by WMISH. In both species, *p58-a* and *p58-b* were expressed only by PMCs. *Sp-p58-a* and *Sp-p58-b* transcripts were not detectable by WMISH prior to hatching (Fig. 2A, B, I and J). Both mRNAs were first detectable at the hatched blastula stage, when they were expressed in the presumptive PMCs (Fig. 2C and K), which form a ring around the small micromeres at the vegetal pole (Fig. 2C and K, inserts). *Sp-p58-a* and *Sp-p58-b* were expressed in ingressed PMCs at the mesenchyme blastula stage (Fig. 2D and L) and uniformly in the PMC syncytium during gastrulation (Fig. 2E, F and M). The level of *Sp-p58-b* declined from the late gastrula stage to the prism stage (Fig. 2N and O) and the mRNA was almost undetectable in pluteus larvae (Fig. 2P). *Sp-p58-a* was expressed at high levels at the prism stage (Fig. 2G). In the pluteus larva, this mRNA was enriched in PMCs in the scheitel (Fig. 2H).

The patterns of expression of *Lv-p58-a* and *Lv-p58-b* were very similar to their *S. purpuratus* orthologs. *Lv-p58-a* and *Lv-p58-b* were undetectable by WMISH prior to hatching (Fig. 3A, B, I and J). At the hatched blastula stage, *Lv-p58-a* was expressed in presumptive PMCs (Fig. 3C, insert), while *Lv-p58-b* was not detectable at this stage (Fig. 3K). *Lv-p58-a* and *Lv-p58-b* mRNAs were restricted to PMCs at the mesenchyme blastula stage (Fig. 3D and L) and were expressed uniformly within the PMC ring during gastrulation (Fig. 3E, F, M and N). *Lv-p58-a* was expressed at high levels at the prism stage (Fig. 3G), and at the pluteus larva stage, was still detectable and appeared to be expressed uniformly in the PMC syncytium (Fig. 3H), unlike *Sp-p58-a* which was enriched in the scheitel at the pluteus stage (Fig. 2H). *Lv-p58-b* mRNA, on the other hand, was not detectable by WMISH at the prism stage or in the pluteus larva (Fig. 3O and P). We noted that at all developmental stages at which the two mRNAs were expressed, *p58-b* was expressed at lower levels than *p58-a*, a difference that was particularly obvious in *L. variegatus* embryos.

Knockdown of P58-A or P58-B causes defects in skeletogenesis in S. purpuratus

We blocked the expression of *p58-a* and *p58-b* in *S. purpuratus* and *L. variegatus* with MOs. Because information on exon/intron boundaries in *S. purpuratus* was available from the genome assembly, we

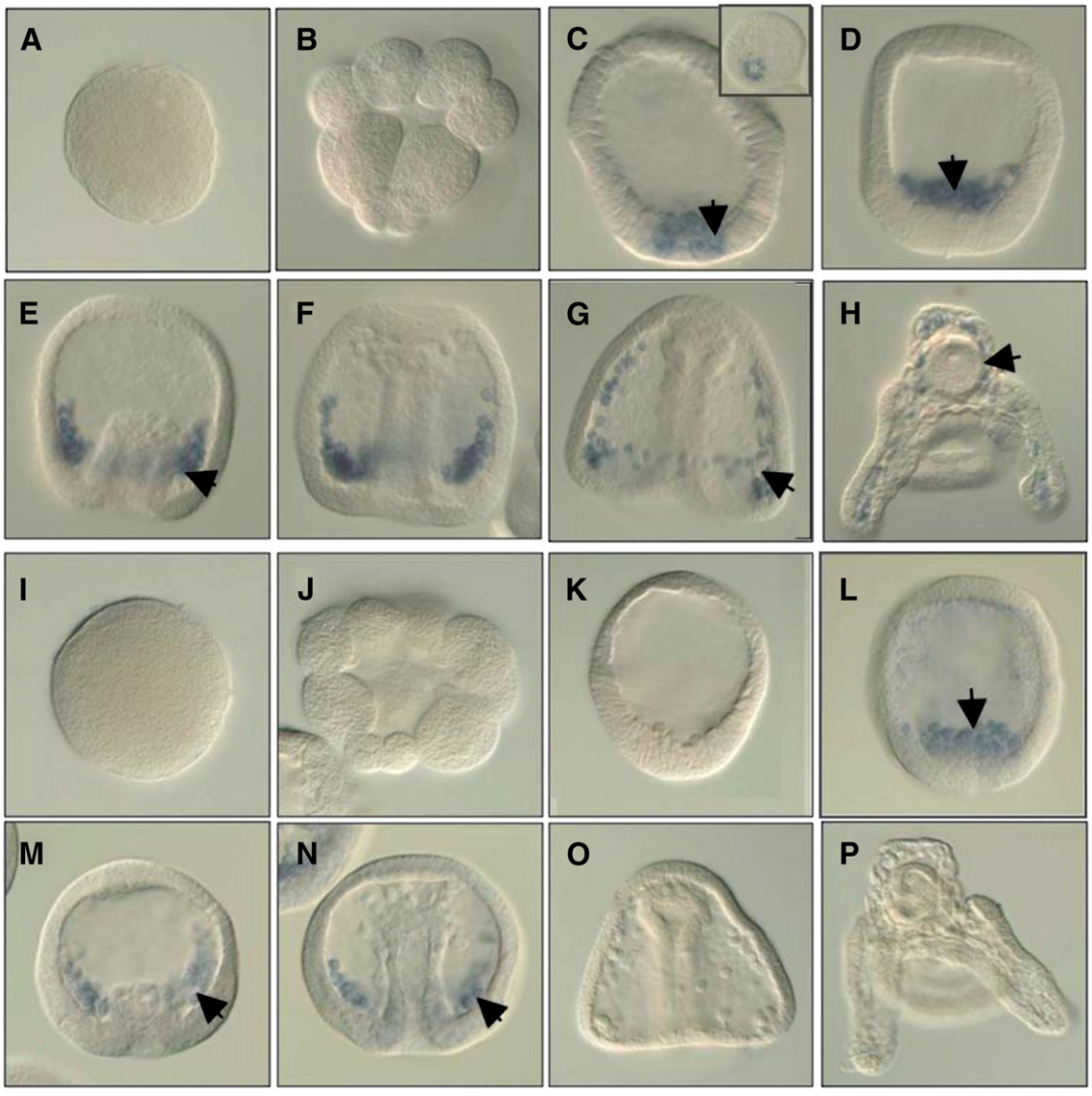

Fig. 3. Whole mount in situ hybridization analysis of *p58-a* (A–H) and *p58-b* (I–P) expression in *L. variegatus*. Expression of *p58-a* is undetectable prior to hatching (A and B). Staining is visible after hatching and is restricted to PMCs throughout later development (arrows, C–H). Expression of *p58-b* is undetectable in stages prior to PMC ingression (I–K). Expression is apparent from the mesenchyme blastula stage through the late gastrula stage (arrows, L–N), after which time expression decreases to undetectable levels (O–P). (A and I) Unfertilized egg. (B and J) 16-cell stage. (C and K) Hatched blastula. (D and L) Mesenchyme blastula. (E and M) Early gastrula. (F and N) Late gastrula. (G and O) Prism. (H and P) Pluteus larva.

used splice-blocking MOs in this species. Splice-blocking MOs are advantageous because it is possible to assess their efficacy by RT-PCR. We designed the *Sp-p58-a* MO to target the exon 3/intron 3 boundary (Fig. 4A). This MO was injected at concentrations of 1, 2, and 4 mM. We extracted RNA from 200 embryos that were injected with MO at each of these concentrations, and RT-PCR analysis was conducted

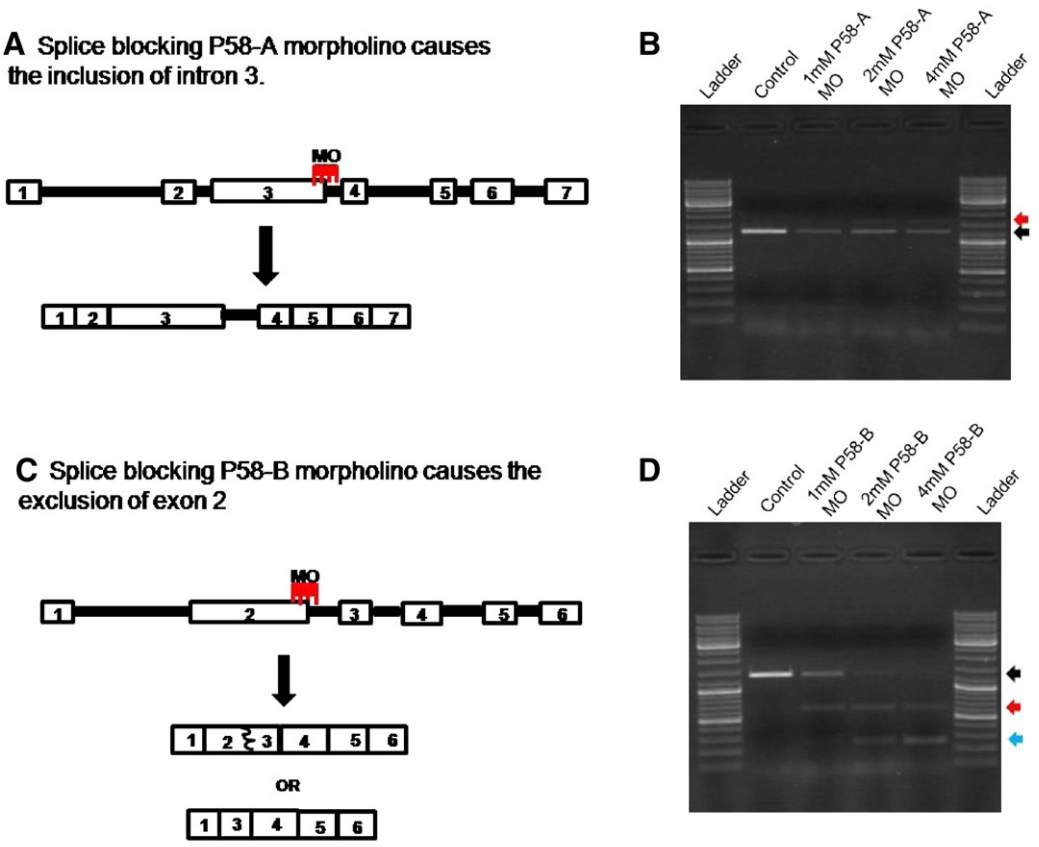

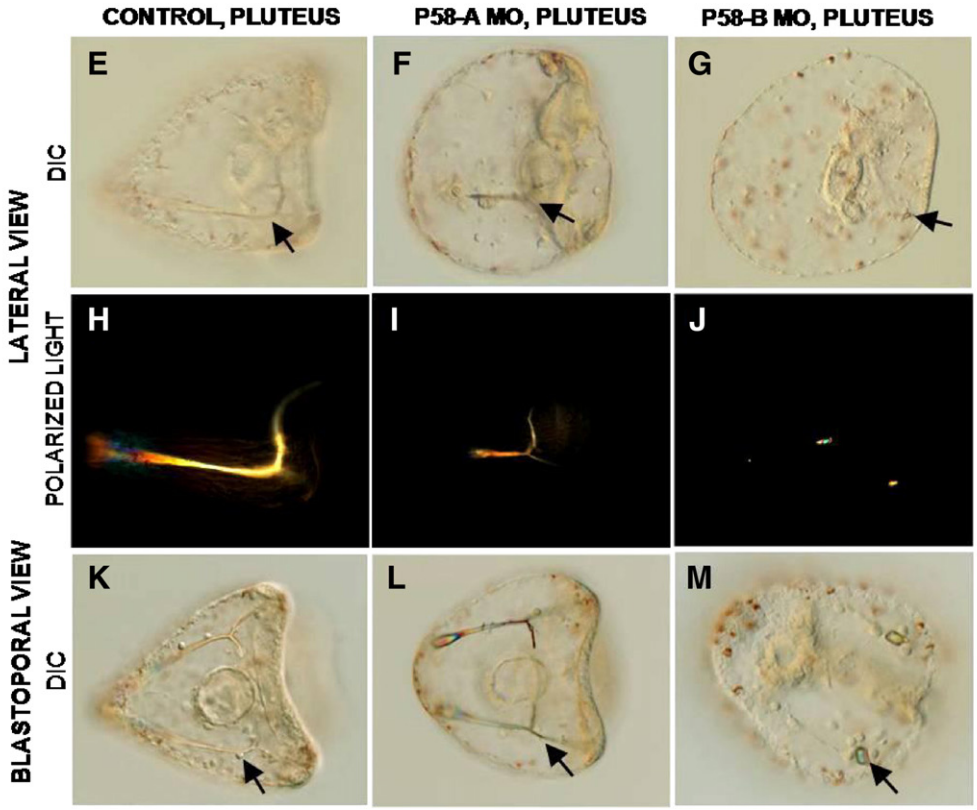

Table 1
Distribution of morphant phenotypes in *S. purpuratus*.

	P58-A morphants (301 embryos)		P58-B morphants (304 embryos)		P58-A/P58-B morphants (300 embryos)	
	#	%	#	%	#	%
No skeletal elements	3	1.0	33	10.9	106	35.3
Unbranched skeletal rudiments	0	0.0	176	57.9	143	47.7
Branched skeletal rudiments	15	5.0	65	21.4	36	12.0
Body rods only	46	15.3	1	0.3	9	3.0
Shortened skeletal rods	237	78.7	29	9.5	6	2.0
Wild type skeleton	0	0.0	0	0.0	0	0.0

using forward and reverse primers that were located in exon 2 and exon 4, respectively. RT-PCR analysis showed that there was a significant decrease in the normal splice form in *Sp-p58-a* MO-injected embryos (Fig. 4B, black arrow). In addition, a band approximately 350 nucleotides larger than the normal splice form appeared in samples extracted from MO-injected embryos (Fig. 4B, red arrow). This larger splice variant was cloned and sequenced, and was shown to have resulted from the inclusion of intron 3, which is 348 nucleotides in length. Inclusion of this intron alters the coding sequence of SpP58-A and introduces a premature stop codon. Embryos injected with 4 mM *Sp-p58-a* MO showed the greatest reduction in the normal splice form of *Sp-p58-a* without any loss in viability (Fig. 4F), and we therefore used this concentration for further experiments. We noted, however, that at all concentrations of *Sp-p58-a* MO, low levels of the normal splice form persisted.

We designed the *Sp-p58-b* MO to be complementary to the exon 2/intron 2 boundary (Fig. 4C). This MO was also tested at concentrations of 1, 2, and 4 mM, and RNA was extracted from 200 embryos for RT-PCR analyses using forward and reverse primers that were located in exons 1 and 3, respectively. We noted that at all three concentrations tested, there was a marked decrease in the level of the normal splice form of *Sp-p58-b* (Fig. 4D, black arrow). We also noted the appearance of two different splice variants, both smaller in size than the control splice form (Fig. 4D). Both of these bands were cloned and sequenced, and this analysis showed that the smallest splice form, which was an estimated 1100 nucleotides smaller than the control splice form (Fig. 4D, blue arrow), was a splice variant that completely lacked exon 2, which is 1110 nucleotides in length. The larger splice variant (Fig. 4D, red arrow) contained approximately the first 700 nucleotides of exon 2, apparently as a consequence of the mobilization of an internal splice site. In both cases, the deletions caused changes in the reading frame of *Sp-p58-b* and introduced premature stop codons. Because injection of 4 mM *Sp-p58-b* MO sometimes resulted in non-specific, toxic effects, we used a concentration of 2 mM for all experiments.

We found that knockdown of either Sp-P58-A and Sp-P58-B caused defects in skeletogenesis. Sp-P58-A morphants had visibly truncated skeletal elements (Fig. 4F, I, and L), though triradiate spicule rudiments were visible at the gastrula stage (data not shown). Morphant embryos had a well-developed gut and numerous pigment cells, and a reduction in the length of the skeletal rods was the only apparent defect (Fig. 4F). We noted that the length and complement of skeletal rods varied among embryos, even within a single batch, though no morphant embryo had fully elongated rods (Table 1). Out of 301 embryos scored, only 1% had no visible skeletal elements. Interestingly, 15.3% of the morphant embryos had only body rods, a phenotype that has not been described following the knockdown of other biomineralization proteins. We also noted that several embryos had severe bifurcations and trifurcations at the tips of the body rods (unpublished data). The vast majority of embryos, 78.7%, had shortened skeletal elements (Table 1).

Although *Sp-p58-b* is expressed at lower levels than *Sp-p58-a*, Sp-P58-B morphants exhibited a more severe phenotype. When control embryos had reached the pluteus stage, the skeleton of most Sp-P58-B morphants consisted of only two, granular deposits of birefringent material (Fig. 4J and M) that were located approximately where the triradiate spicule rudiments would ordinarily form. These deposits were not triradiate in shape, but rather rod-shaped (Fig. 4J) or rectangular (Fig. 4M). Though there were no elongated skeletal rods in Sp-P58-B morphants, cells that appeared to be PMCs were visible by differential interference contrast (DIC) microscopy and these cells were linked to each other by filopodial cables in the stereotypical pattern of the PMC syncytium. Sp-P58-B morphants did not exhibit any other developmental defects (Fig. 4G and M). Out of 304 Sp-P58-B morphant embryos scored, 10% formed no skeletal elements (Table 1). 57.9% formed unbranched skeletal rudiments, and another 21.4% formed abnormal, branched skeletal rudiments (Table 1). As with Sp-P58-A morphants, no Sp-P58-B morphants had a wild-type skeleton. Sp-P58-A and Sp-P58-B morphant embryos both had a more rounded shape than sibling control embryos, as a secondary consequence of defects in skeletal rod elongation (Fig. 4F, L, G and M).

Double knockdown of Sp-P58-A and Sp-P58-B almost completely blocks skeletogenesis

Because knockdowns of Sp-P58-A and Sp-P58-B individually both impaired skeletal development, we concluded that these two proteins are not completely redundant, despite their striking structural similarity. It is possible, however, that P58-A and P-58B have similar biochemical functions in vivo and that, in the absence of either protein, the other is capable of supporting skeletogenesis, albeit in a compromised fashion. This could explain our finding that skeletogenesis was partially, but not completely suppressed, both in Sp-P58-A and Sp-P58-B morphants.

To explore the possibility that the proteins have partially overlapping functions, we tested whether a double knockdown of both Sp-P58-A and Sp-P58-B would result in a more complete inhibition of skeletal development. We injected embryos with a solution that contained both the Sp-P58-A and Sp-P58-B MOs, each at a concentration of 2 mM. The skeletal defects that we observed were more severe than for a single knockdown of either Sp-P58 protein, although most double knockdown embryos still produced small skeletal elements (Fig. 5, Table 1). In 300 double knockdown embryos scored, 35.3% had no skeletal elements, a percentage higher than for

Fig. 4. Knockdown of P58-A and P58-B in *S. purpuratus* using splice-blocking morpholinos (MOs) suppresses skeletogenesis. (A) Schematic of the design of *Sp-p58-a* splice-blocking MO. (B) Agarose gel showing the depletion of the correctly spliced form of *Sp-p58-a* (black arrow), and the accumulation of a larger, misspliced variant that contains intron 3 (red arrow). (C) Schematic of the design of *Sp-p58-b* splice-blocking MO. (D) Agarose gel showing the depletion of the correctly spliced form of *Sp-p58-b* (black arrow) and the accumulation of two misspliced variants that lack part or all of exon 2 (red and blue arrows, respectively). (E–G) DIC and (H–J) polarized light images of lateral views of control and morphant embryos at the pluteus stage. (K–M) DIC images of blastoporal views of control and morphant embryos at the pluteus stage. (E, H, and K) Control embryos. (F, I, and L) P58-A morphants. (G, J, and M) P58-B morphants. Skeletal elements (arrows) are reduced in P58 morphant embryos, and this effect is most pronounced in the case of P58-B morphants.

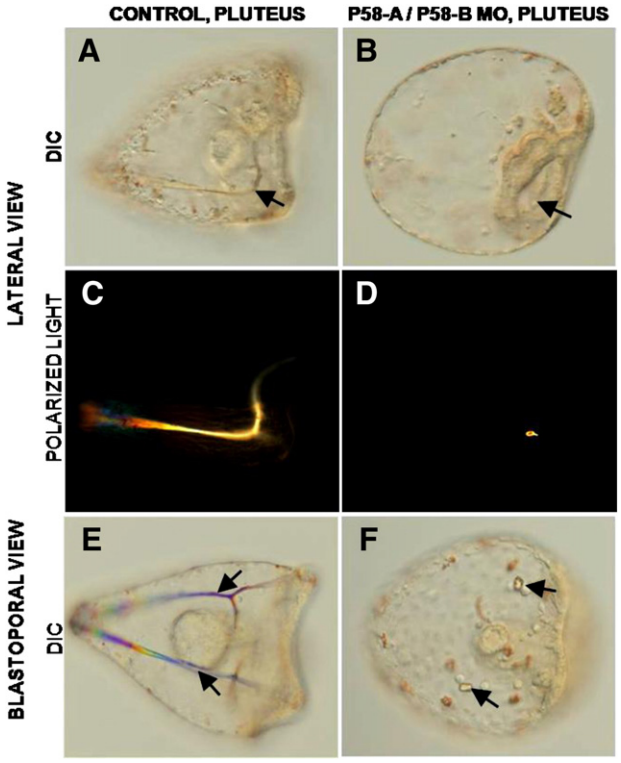

Fig. 5. Double knockdown of P58-A and P58-B in *S. purpuratus* almost completely suppresses skeletogenesis. (A and B) DIC and (C and D) polarized light images of lateral views of control and morphant embryos. (E and F) DIC images of blastoporal views of control and morphant embryos. (A, C, and E) Control embryos. (B, D, and F) P58-A/P58-B morphants. In most double knockdown embryos at the pluteus stage, no skeletal elements, or only one or two tiny granules of birefringent material (arrows), are present.

Sp-P58-A or Sp-P58-B morphant embryos, of which only 1% and 10.9% of morphants formed no skeletal elements, respectively (Table 1). 47.7% of double morphant embryos had unbranched skeletal rudiments (Fig. 5B, D, and F and Table 1). Unlike Sp-P58-B morphants, which had symmetrical rudiments, Sp-P58-A/Sp-P58-B double knockdown embryos often had a single, tiny skeletal rudiment (data not shown). Double knockdown of Sp-P58-A and Sp-P58-B therefore resulted in a more complete suppression of skeletogenesis than either single knockdown, a finding which is consistent with the view that the proteins act in an additive fashion to mediate skeletogenesis. The fact that some skeletal material was still deposited in most double knockdown embryos might suggest that P58-A and P58-B do not play a role in the initiation of spicule deposition; more likely, however, this finding reflects the fact that our MOs were not 100% effective at blocking the expression of these proteins.

Knockdowns of P58-A and P58-B cause skeletal defects in L. variegatus

We found that the amino acid sequences of Lv-P58-A and Lv-P58-B were very similar to those of their *S. purpuratus* homologs (Fig. 1). To validate the functional studies that we carried out in *S. purpuratus*, and to test whether P58-A and P58-B have similar roles in other species, P58 knockdown experiments were also carried out in *L. variegatus*. We designed an *Lv-p58-a* translation-blocking MO and injected this into fertilized eggs at a concentration of 0.5 mM. Lv-P58-A morphants exhibited a phenotype that was very similar to that of Sp-P58-A morphants. In these embryos, most major skeletal rods were present and their arrangement appeared relatively normal, though these rods were severely truncated (Fig. 6B and F). Lv-P58-B morphants also had a phenotype that resembled *S. purpuratus* morphants. Embryos that were injected with an *Lv-p58-b* translation-blocking MO at a concentration of 0.1 mM had severely perturbed skeletons; >90% of these embryos formed only two small deposits of skeletal material (Fig. 6C and G). Lv-P58-A and Lv-P58-B morphants showed no visible developmental defects that were unrelated to the extension of skeletal rods (Fig. 6B and C).

We also tested the effect of a knockdown of both P58 proteins in *L. variegatus* by injecting fertilized eggs with a solution that contained *Lv-p58-a* and *Lv-p58-b* MOs at concentrations of 0.5 and 0.1 mM, respectively. In this experiment also, the phenotypes of *L. variegatus* embryos closely resembled those of *S. purpuratus* embryos after a similar perturbation. Lv-P58-A/Lv-P58-B double morphant embryos formed only very small deposits of skeletal material that were visible under polarized light (Fig. 6D and H). As with double knockdown embryos in *S. purpuratus*, we observed some cases in which only one granule of skeletal material was visible in these double knockdown embryos (data not shown). These functional studies, carried out in two sea urchin species using MOs with different characteristics (e.g., splice-blocking versus translation-blocking) and different sequences, show that P58-A and P58-B both play important roles in skeletogenesis, although P58-B may have a more critical function.

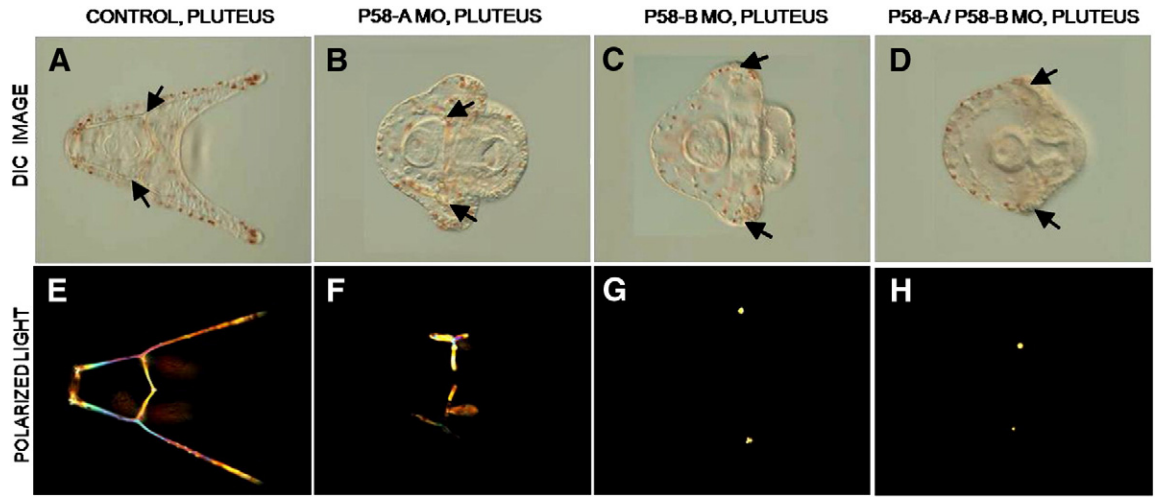

Fig. 6. Knockdown of P58-A or P58-B inhibits skeletogenesis in *L.* variegatus. (A–D) DIC and (E–H) polarized light images of control and morphant embryos. Blastoporal views of control embryos (A and E), P58-A morphants (B and F), P58-B morphants (C and G), and P58-A/P58-B morphants (D and H) at the pluteus stage. Skeletal elements (arrows) are reduced in P58 morphant embryos; this effect is more pronounced in the case of P58-B morphants than in P58-A morphants.

P58-A and P58-B do not regulate PMC specification or migration

Because skeletal morphogenesis was clearly perturbed following knockdown of P58-A and/or P58-B, we tested whether PMCs were specified and migrated correctly under these conditions. At the late gastrula stage (Fig. 7A–H), we used P19, which is expressed only by PMCs, as a differentiation marker (Illies et al., 2002). We found that PMCs were specified correctly both in Sp-P58-A and Sp-P58-B morphants (Fig. 7B, F, C and G). WMISH analysis showed that Sp-P19 was expressed on schedule and in a pattern similar to that observed in control embryos. It was also evident that PMCs in morphant embryos were arranged in a stereotypical, subequatorial

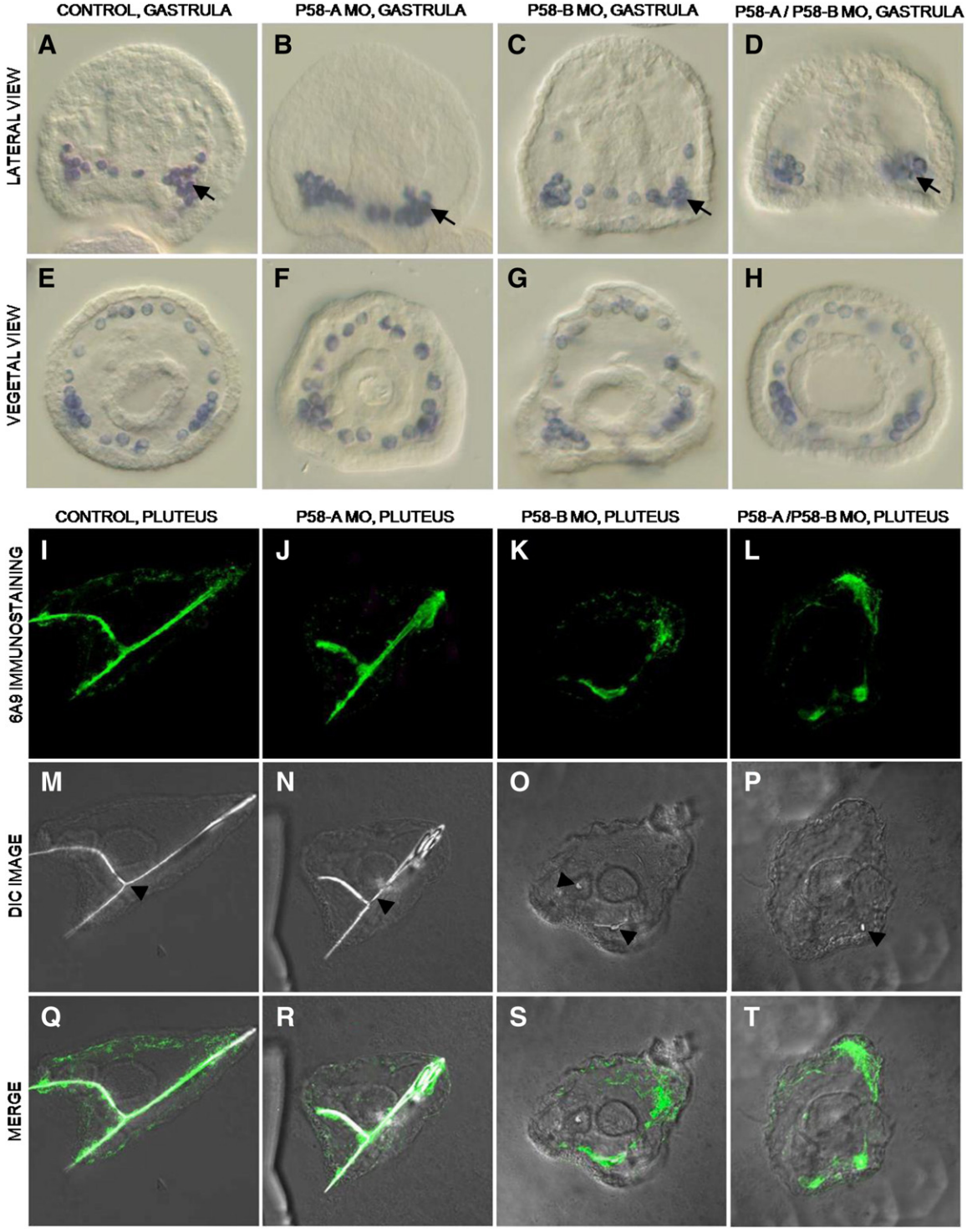

Fig. 7. Knockdown of P58-A and P58-B does not inhibit PMC specification or migration in *S. purpuratus.* (A–H)Whole mount in situ hybridization with a *p19* probe, showing the distribution of PMCs (arrows) at the gastrula stage. (A–D) Lateral view and (E–H) vegetal views of control (A and E), P58-A morphants (B and F), P58-B morphants (C and G), and P58-A/P58-B double knockdown embryos (D and H). The number and distribution of PMCs are similar in control and morphant embryos. The expression of *p19*, a late marker, suggests that the specification of the PMCs is unaffected. At the pluteus stage (I–T), 6a9 immunostaining, which recognizes MSP130 proteins, shows comparable PMC positioning in control embryos (I, M, and Q), P58-A morphants (J, N, and R), P58-B morphants (K, O, and S), and P58-A/P58-B double knockdown embryos (L, P, and T), even in the absence of well formed skeletal elements. Skeletal elements are indicated by arrowheads.

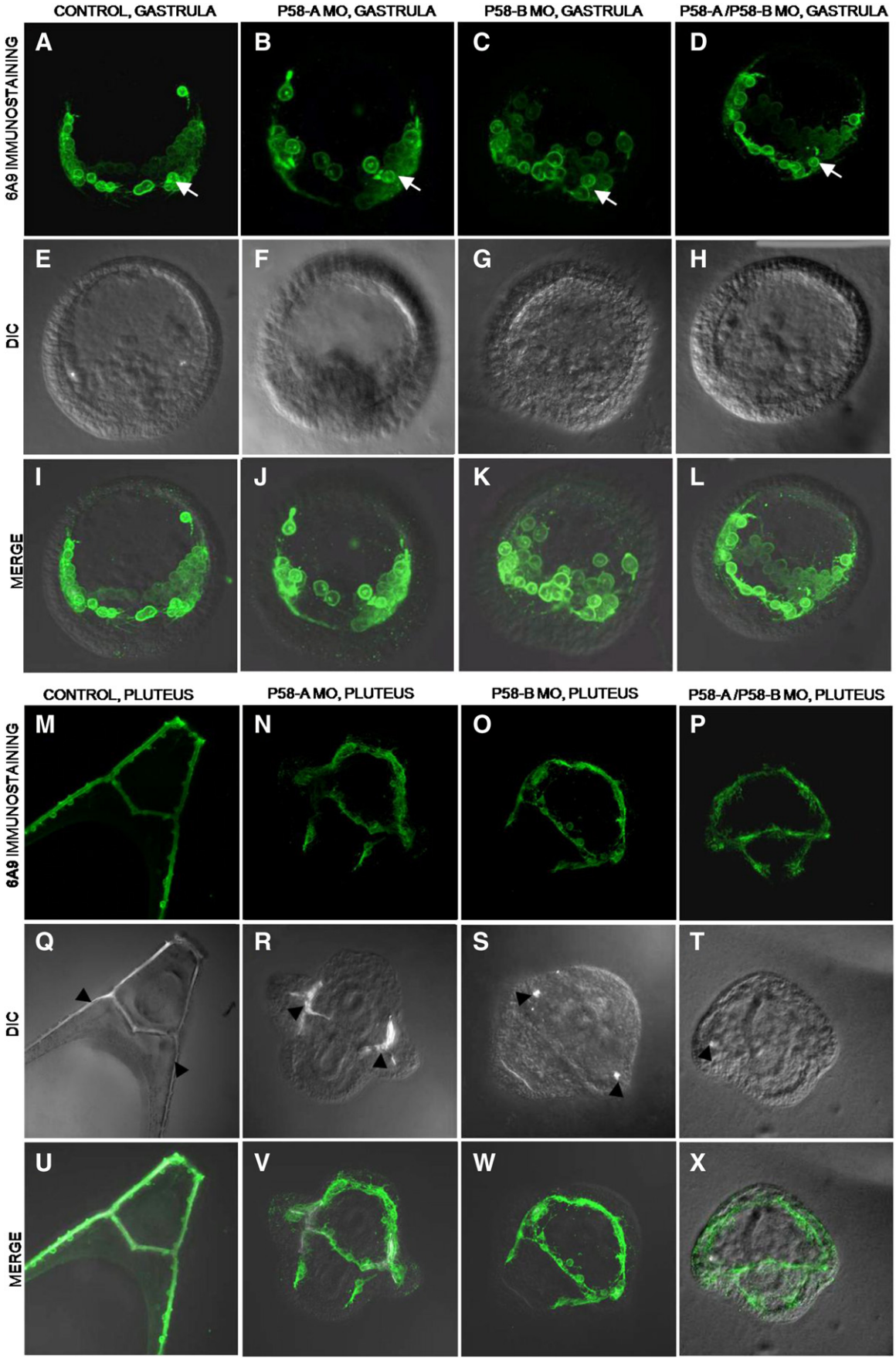
CONTROL, GASTRULA
P58-A MO, GASTRULA
P58-B MO, GASTRULA
P58-A /P58-B MO, GASTRULA
6A9 IMMUNOSTAINING
DIC
MERGE
A
B
C
D
E
F
G
H
I
J
K
L
CONTROL, PLUTEUS
P58-A MO, PLUTEUS
P58-B MO, PLUTEUS
P58-A /P58-B MO, PLUTEUS
6A9 IMMUNOSTAINING
DIC
MERGE
M
N
O
P
Q
R
S
T
U
V
W
X

ring pattern. The two ventrolateral clusters of the subequatorial ring were clearly visible and were connected by oral and aboral chains of PMCs (Fig. 7F and G). There were also no observable defects in PMC specification and migration in Sp-P58-A/Sp-P58-B double knockdown embryos, and the subequatorial PMC ring appeared to be patterned normally in these morphants (Fig. 7D and H). We also examined the organization of PMCs late in development (i.e., at the pluteus larva stage) using the monoclonal antibody 6a9, which recognizes a family of PMC-specific surface glycoproteins (Fig. 7I–T). In pluteus larvae, skeletal elements are highlighted with this antibody, which stains the PMC filopodial cables that surround the skeletal rods (Fig. 7A). In Sp-P58-A knockdown embryos, the 6a9 antibody stained PMC filopodial cables and PMC cell bodies that were associated with skeletal rods (Fig. 7J), in a manner similar to control embryos (Fig. 7I). Unlike Sp-P58-A morphants which have relatively well defined skeletal elements (Figs. 4I and 7N), Sp-P58-B morphants deposit very small amounts of skeletal material (Figs. 4J and 7O). In Sp-P58-B morphants at the pluteus stage, we found that although there were no extended skeletal rods (as indicated by the black arrows in Fig. 7O), PMCs were localized in a pattern that was indistinguishable from that observed in control embryos and Sp-P58-A morphants. Thus, in P58-B morphants, PMCs pattern themselves correctly at later stages of development even in the absence of skeletal rods (Fig. 7K, O, and S). This was also the case in Sp-P58-A/Sp-P58-B double knockdown embryos (Fig. 7L, P, and T).

We assayed the presence and location of PMCs in *L. variegatus* P58 morphants at the gastrula stage. 6a9 immunostaining showed that PMCs were present in Lv-P58-A and Lv-P58-B morphants and these cells formed a subequatorial ring with two ventrolateral clusters that were joined by oral and aboral chains of PMCs (Fig. 8B, J, C, and K). We also determined that PMCs were correctly specified and patterned in Lv-P58-A/Lv-P58-B double knockdown embryos (Fig. 8D and L). At the pluteus larva stage, control embryos clearly showed 6a9 immunostaining throughout the skeleton, with PMC cell bodies positioned along the extended skeletal rods (Fig. 8M and U). The PMC syncytium was clearly visible in Lv-P58-A and Lv-P58-B morphants (Fig. 8N and O). PMC cables and cell bodies were found in locations similar to the location of PMCs in control embryos, though skeletal rods were severely shortened in Lv-P58-A morphants (Fig. 8R and V), and only small deposits of biomineral were present in Lv-P58-B morphants (Fig. 8S and W). We observed similar effects in Lv-P58-A/Lv-P58-B double knockdown embryos, (Fig. 8P, T, and X). Thus, we detected no defects in the specification and migration of PMCs in P58 knockdown embryos, either in *S. purpuratus* or *L. variegatus*.

P58-A and P58-B do not regulate PMC fusion

PMC fusion may be required in order to produce an expansive, "privileged" extracellular space within which spicule elongation can occur (Wilt and Ettensohn, 2007). We used a dye-transfer assay to test the ability of individual PMCs to undergo fusion following knockdown of P58-A or P58-B. Two to six PMCs were removed from an Lv-P58-A morphant embryo that had been labeled with fluorescein dextran, and these cells were transplanted into a host embryo that had been injected with Lv-P58-A MO without dextran (see Materials and methods). It was shown previously that in control embryos, PMCs that contain dextran transfer the label to cells throughout the syncytium as a consequence of cell fusion (Hodor and Ettensohn, 1998; 2008). We observed in 7 out of 7 cases that dextran-labeled PMCs from Lv-P58-A morphants fused with PMCs of the unlabeled host embryo, as indicated by the spread of the dextran throughout the PMC syncytium (Fig. 9A and E). All host embryos also displayed the characteristic Lv-P58-A knockdown phenotype of severely shortened skeletal rods (Fig. 9C). This experiment was repeated for Lv-P58-B morphant embryos, in which case 13 out of 13 embryos showed fusion of dextran-labeled cells with the host PMC syncytium (Fig. 9B and F). 12 out of these 13 embryos showed the morphant phenotype of greatly reduced skeletal deposits (Fig. 9D). These studies strongly suggest that P58-A and P58-B are not required for PMC fusion in the sea urchin embryo. They are consistent with our observation that extensive filopodial cables form in morphant embryos, even in areas where no spicule material is deposited.

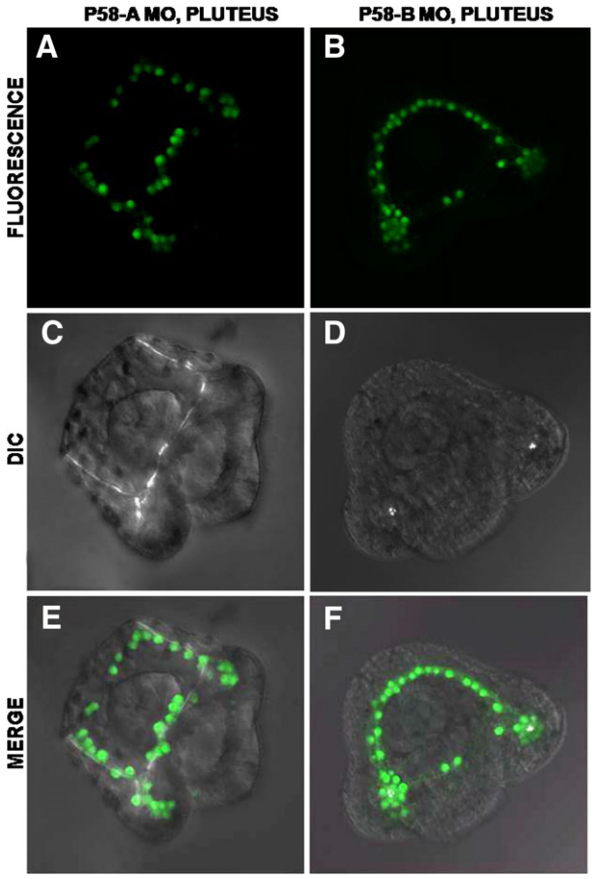

Fig. 9. PMC fusion is not perturbed in P58-A (A, C, and E) and P58-B (B, D, and F) morphants. Fluorescence (A and B), DIC (C and D), and merged (E and F) images of unlabeled, morpholino-injected *L. variegatus* embryos into which a small number of PMCs from a dextran-labeled, morpholino-injected embryo were introduced. PMCs in P58-A and P58-B morphants are fusion-competent, as indicated by the diffusion of dextran throughout the PMC syncytium.

Discussion

The embryonic skeleton of the sea urchin is the primary determinant of the overall shape of the late embryo and the larva. This complex anatomical structure is secreted by specialized, biomineral-forming cells (PMCs), the activities of which are tightly regulated by cues provided by overlying epithelial cells (Wilt and Ettensohn, 2007). Based upon the recent elucidation of the PMC GRN, and a large body of work concerning the cell biological and embryological basis of skeletogenesis in the sea urchin, it should soon be possible to develop a relatively complete understanding of the genomic regulatory control of this major

Fig. 8. Knockdown of P58-A and P58-B does not inhibit PMC specification or migration in *L. variegatus*. 6a9 immunostaining reveals the presence and location of PMCs (arrows) at the gastrula stage (A–L). Fluorescence (A–D), DIC (E–H), and merged (I–L) images show comparable positioning of PMCs in *L. variegatus* control embryos (A, E, and I), P58-A morphants (B, F, and J), P58-B morphants (C, G, and K), and P58-A/P58-B double knockdown embryos (D, H, and L). At the pluteus stage (M–X), PMCs and filopodial cables (arrowheads) are present in comparable positions in control embryos (M, Q, and U), P58-A morphants (N, R, and V), P58-B morphants (O, S, and W), and P58-A/P58-B double knockdown embryos (P, T, and X), even in the absence of well formed skeletal elements (arrowheads). The expression of MSP130 proteins, which are recognized by the 6a9 antibody, suggests that the specification of the PMCs is unaffected.

morphogenetic process. This, in turn, will provide a basis for understanding the genomic and embryological changes that have accompanied the evolutionary modification of skeletal development within the echinoderms, a phylum that exhibits remarkably diverse patterns of skeletogenesis. An important component of this analysis will be the identification and functional analysis of proteins that play direct roles in each of the various phases of skeletal morphogenesis, including biomineral deposition. Although numerous proteins have been implicated in biomineralization based upon patterns of expression and/or conserved sequence features, there have been few studies that have demonstrated the functional importance of specific, candidate biomineralization proteins, e.g., by gene knockdown approaches (Peled-Kamar et al., 2002; Cheers and Ettensohn, 2005 ; Wilt et al., 2008b).

We have shown that two novel PMC-specific proteins, P58-A and P58-B, play essential roles in skeletogenesis. Knockdown of either protein using splice-blocking or translation-blocking MOs impairs biomineral deposition but does not affect PMC specification, ingression, directional migration, or fusion. Our findings therefore indicate that P58-A and P58-B function as terminal biomineralization proteins. The critical role of these proteins in biomineralization has been conserved for at least 100 Ma, i.e., the approximate divergence time between *L. variegatus* and *S. purpuratus* (Smith et al., 2006). An ongoing analysis of the regulatory control of biomineralization genes has identified some of the transcriptional inputs into *p58-a* and *p58-b*; for example, both genes receive a positive input from *ets1* and neither is regulated by *t-brain*, but only *p58-a* receives a positive input from *alx1* (Rafiq and Ettensohn, unpublished observations).

Despite the similarities between P58-A and P58-B, MO knockdown studies indicate that the two proteins are not fully redundant. In both species that we have examined, MO knockdown of either P58-A or P58-B leads to an inhibition of skeleton deposition. Knockdown of P58-B, however, consistently results in a more severe suppression of skeleton deposition. Perhaps paradoxically, WMISH data indicate that *p58-b* is expressed at lower levels than *p58-a* throughout development. This observation is supported by recent QPCR studies which show that the number of *Sp-p58-a* transcripts/cell is approximately 10 times greater than the number of *Sp-p58-b* transcripts/cell (Rafiq and Ettensohn, unpublished observations). The high level of *p58-a* transcripts may make it more difficult to completely suppress gene function using MOs, at least at MO concentrations that do not cause a loss of embryo viability. Indeed, our RT-PCR analysis indicated that a greater proportion of the targeted transcript was spliced normally in the presence of the *Sp-p58-a* splice-blocking MO than in the case of the *Sp-p58-b* splice-blocking MO (Fig. 4). It is also possible, however, that despite their similar sequences and their different levels of mRNA expression, *p58-B* plays a more critical role in biomineral deposition than does *p58-A*.

P58-A and P58-B are novel proteins and their sequences provide few clues concerning their biochemical function(s). Both proteins contain an N-terminal signal sequence and a single transmembrane domain. Several basic residues lie immediately C-terminal to the transmembrane domain and probably function as a stop-transfer signal. This organization suggests that P58-A and P58-B are synthesized on the rough endoplasmic reticulum and enter the secretory pathway as single-pass, type I transmembrane proteins. Support for this view also comes from the finding that a GFP-tagged form of P58-A is localized primarily within the plasma membrane (Ettensohn, unpublished observations). With the exception of Lv-P58-A, the P58 proteins have extremely short cytoplasmic domains that consist of only the basic, stop-transfer sequence. It therefore seems very likely that the much larger ectodomain plays an important role in the function of these proteins. One possibility is that the P58 ectodomain is released from the membrane by proteolysis and incorporated directly into the biomineral. A recent mass spectrophotometric analysis of the proteome of purified spicules has identified more than 200 proteins, including P58-A, P58-B, and several other transmembrane proteins that have large ectodomains (Mann et al., 2010b). It has been proposed that the ectodomains of many of these proteins are cleaved by matrix metalloproteases, which are also abundant in the spicule matrix. The same study also identified a number of cytoplasmic proteins, such as ribosomal proteins and translation factors, in purified spicules, and therefore some artifactual redistribution of proteins occurred during sample preparation. Nevertheless, these findings support a model which suggests that, at some stage in the secretory pathway, the ectodomains of P58-A and P58-B are cleaved, and are later released into the extracellular space and incorporated into the biomineral. The mass of the spicule is overwhelmingly mineral (mostly $CaCO_3$, in the form of calcite), but the small amounts of occluded proteins are thought to play a critical role in regulating the assembly and physical properties of the material (Wilt and Ettensohn, 2007). We can only speculate concerning the possible function of the P58 ectodomain in biomineralization; for example, it might play a role in stabilizing amorphous calcium carbonate or in converting it to a crystalline state, or it might function in regulating the transport of calcium or other biomineralization proteins inside the cell (Politi et al., 2008; Wilt et al., 2008a).

The phenotypes of P58-A and P58-B morphants are reminiscent of those observed following MO knockdown of P16, another novel protein involved in biomineralization (Cheers and Ettensohn, 2005). Like P58-A and P58-B, P16 is a type I transmembrane protein with an N-terminal signal sequence and a C-terminal transmembrane domain (Illies et al., 2002). Also like the P58 proteins, P16 has apparently undergone recent duplication, as this gene is clustered near several very closely related genes (Livingston et al., 2006). The ectodomain of P16, however, appears quite different from that of P58; it is acidic and contains a high proportion of serine and aspartate residues. As in the case of P58-A and P58-B, MO knockdown of P16 greatly suppresses, but does not completely block, the deposition of biomineral. There may be technical reasons for this, such as the incomplete knockdown of the target proteins. It seems very likely, however, that the many genes that mediate biomineralization have overlapping and therefore partially redundant functions. Further work will be necessary to distinguish between the possible modes of function of the P58 proteins to explore their potential interactions with other biomineralization proteins.

Although biomineralization evolved independently in echinoderms and vertebrates, the genes that encode secreted biomineralization proteins have undergone extensive duplication in both taxa. Whole genome duplication as well as local, tandem gene duplications have been important in the evolution of several families of extracellular biomineralization proteins in vertebrates (reviewed by Kawasaki et al., 2009). In sea urchins, members of the spicule matrix, MSP130, and P16 protein families are found in small clusters (Livingston et al., 2006). Higher order clustering of these genes is probably obscured by the relatively small size of the scaffolds in the current *S. purpuratus* genome assembly. In the present study, we have found that P58-A and P58-B lie side by side in the genome. Although the exon–intron organization of these genes is not identical (Fig. 1A), their similar amino acid sequences and tandem arrangement indicate that either *p58-a* or *p58-b* arose as a duplication of the other gene (Hahn, 2009, Lee et al., 2007). This hypothesis is also supported by the observation that P58-A and P58-B have similar, yet non-redundant roles, a trademark of duplicated genes (Innan and Kondrashov, 2010). The duplication of the ancestral *p58* gene clearly predated the last common ancestor of *L. variegatus* and *S. purpuratus*. A more complete reconstruction of the evolutionary history of the *p58* genes, and of the other sea urchin biomineralization genes, will be possible once additional echinoderm genome assemblies become available.

Acknowledgments

This work was supported by N.S.F. Grants IOS-0745875 and IOS-1021805 to C.A.E. The authors thank Dr. Cynthia Bradham and Dr. Albert Poustka, who generously provided Lv-P58-B cDNA sequences, and Trevor Ellison, who synthesized the *Sp-p58-b* WMISH probe.

References

Benson, S., Sucov, H., Stephens, L., Davidson, E., Wilt, F., 1987. A lineage-specific gene encoding a major matrix protein of the sea urchin embryo spicule I. Authentication of the cloned gene and its developmental expression. Dev Biol. 120, 499–506.

Cheers, M.S., Ettensohn, C.A., 2004. Rapid microinjection of fertilized eggs. In: Ettensohn, C.A., Wessel, G.M., Wray, G.A. (Eds.), Development of sea urchins, ascidians, and other invertebrate deuterostomes: experimental approaches. Meth. Cell Biol. 74, 287–310.

Cheers, M.S., Ettensohn, C.A., 2005. P16 is an essential regulator of skeletogenesis in the sea urchin embryo. Dev. Biol. 283, 384–396.

Croce, J., Lhomond, G., Lozano, J.C., Gache, C., 2001. Ske-T, a T-box gene expressed in the skeletogenic mesenchyme lineage of the sea urchin embryo. Mech. Dev. 107, 159–162.

Cserzö, M., Wallin, E., Simon, I., von Heijne, G., Elofsson, A., 1997. Prediction of transmembrane alpha-helices in prokaryotic membrane proteins: the dense alignment surface method. Protein Eng. 10, 673–676.

Duloquin, L., Lhomond, G., Gache, C., 2007. Localized VEGF signaling from ectoderm to mesenchyme cells controls morphogenesis of the sea urchin embryo skeleton. Development 134, 2293–2302.

Emanuelsson, O., Brunak, S., von Heijne, G., Nielsen, H., 2007. Locating proteins in the cell using TargetP, SignalP, and related tools. Nat. Protoc. 2, 953–971.

Ettensohn, C.A., McClay, D.R., 1988. Cell lineage conversion in the sea urchin embryo. Dev. Biol. 125, 396–409.

Ettensohn, C.A., Malinda, K.M., 1993. Size regulation and morphogenesis: a cellular analysis of skeletogenesis in the sea urchin embryo. Development 119, 155–167.

Ettensohn, C.A., Illies, M.R., Oliveri, P., De Jong, D.L., 2003. Alx1, a member of the Cart1/Alx3/Alx4 subfamily of Paired-class homeodomain proteins, is an essential component of the gene network controlling skeletogenic fate specification in the sea urchin embryo. Development 130, 2917–2928.

Ettensohn, C.A., 2009. Lessons from a gene regulatory network: echinoderm skeletogenesis provides insights into evolution, plasticity and morphogenesis. Development 136, 11–21.

Fuchikami, T., Mitsunaga-Nakatsubo, K., Amemiya, S., Hosomi, T., Watanabe, T., Kurokawa, D., Kataoka, M., Harada, Y., Satoh, N., Kusunoki, S., Takata, K., Shimotori, T., Yamamoto, T., Sakamoto, N., Shimada, H., Akasaka, K., 2002. T-brain homologue (HpTb) is involved in the archenteron induction signals of micromere descendant cells in the sea urchin embryo. Development 129, 5205–5216.

George, N.C., Killian, C.E., Wilt, F.H., 1991. Characterization and expression of a gene encoding a 30.6-kDa Strongylocentrotus purpuratus spicule of matrix protein. Dev. Biol. 147, 334–342.

Gustafson, T., Wolpert, L., 1961. Studies on the cellular basis of morphogenesis in the sea urchin embryo. Directed movements of primary mesenchyme cells in normal and vegetalized larvae. Exp Cell Res. 24, 64–79.

Hahn, M.W., 2009. Distinguishing among evolutionary models for the maintenance of gene duplicates. J. Hered. 100, 605–617.

Harkey, M.A., Klueg, K., Sheppard, P., Raff, R.A., 1995. Structure, expression, and extracellular targeting of PM27, a skeletal protein associated specifically with growth of the sea urchin larval spicule. Dev. Biol. 168, 549–566.

Hodor, P.G., Ettensohn, C.A., 1998. The dynamics and regulation of mesenchymal cell fusion in the sea urchin embryo. Dev. Biol. 199, 111–124.

Hodor, P.G., Ettensohn, C.A., 2008. Mesenchymal cell fusion in the sea urchin embryo. Meth. Mol. Biol. 475, 315–334.

Illies, M.R., Peeler, M.T., Dechtiaruk, A.M., Ettensohn, C.A., 2002. Identification and developmental expression of new biomineralization proteins in the sea urchin Strongylocentrotus purpuratus. Dev. Genes Evol. 212, 419–431.

Innan, H., Kondrashov, F., 2010. The evolution of gene duplications: classifying and distinguishing between models. Nat. Rev. Genet. 11, 97–108.

Kawasaki, K., Buchanan, A.V., Weiss, K.M., 2009. Biomineralization in humans: making the hard choices in life. Annu. Rev. Genet. 43, 119–142.

Kurokawa, D., Kitajima, T., Mitsunaga-Nakatsubo, K., Amemiya, S., Shimada, H., Akasaka, K., 1999. HpEts, an ets-related transcription factor implicated in primary mesenchyme cell differentiation in the sea urchin embryo. Mech. Dev. 80, 41–52.

Lee, Y., Britten, R.J., Davidson, E.H., 1999. SM37, a skeletogenic gene of the sea urchin embryo linked to the SM50 gene. Dev. Growth Differ. 41, 303–312.

Lee, J.A., Carvalho, C.M., Lupski, J.R., 2007. A DNA replication mechanism for generating nonrecurrent rearrangements associated with genomic disorders. Cell 131, 1235–1247.

Lepage, T., Sardet, C., Gache, C., 1992. Spatial expression of the hatching enzyme gene in the sea urchin embryo. Dev. Biol. 150, 23–32.

Livingston, B.T., Killian, C.E., Wilt, F., Cameron, A., Landrum, M.J., Ermolaeva, O., Sapojnikov, V., Maglott, D.R., Buchanan, A.M., Ettensohn, C.A., 2006. A genome-wide analysis of biomineralization-related proteins in the sea urchin Strongylocentrotus purpuratus. Dev. Biol. 300, 335–348.

Malinda, K.M., Fisher, G.W., Ettensohn, C.A., 1995. Four-dimensional microscopic analysis of the filopodial behavior of primary mesenchyme cells during gastrulation in the sea urchin embryo. Dev. Biol. 172, 552–566.

Mann, K., Poustka, A.J., Mann, M., 2008. In-depth, high-accuracy proteomics of sea urchin tooth organic matrix. Proteome Sci. 6, 33.

Mann, K., Poustka, A.J., Mann, M., 2010a. Phosphoproteomes of Strongylocentrotus purpuratus shell and tooth matrix: identification of a major acidic sea urchin tooth phosphoprotein, phosphodontin. Proteome Sci. 8, 6.

Mann, K., Wilt, F.H., Poustka, A.J., 2010b. Proteomic analysis of sea urchin (Strongylocentrotus purpuratus) spicule matrix. Proteome Sci. 8, 33.

Miller, J., Fraser, S.E., McClay, D., 1995. Dynamics of thin filopodia during sea urchin gastrulation. Development 121, 2501–2511.

Okazaki, K., 1975. Normal development to metamorphosis. In: Czihak, G. (Ed.), The Sea Urchin Embryo. Springer-Verlag, New York, pp. 177–232.

Oliveri, P., Carrick, D.M., Davidson, E.H., 2002. A regulatory gene network that directs micromere specification in the sea urchin embryo. Dev. Biol. 246, 209–228.

Oliveri, P., Tu, Q., Davidson, E.H., 2008. Global regulatory logic for specification of an embryonic cell lineage. Proc. Natl Acad. Sci. USA 105, 5955–5962.

Peled-Kamar, M., Hamilton, P., Wilt, F.H., 2002. Spicule matrix protein LSM34 is essential for biomineralization of the sea urchin spicule. Exp. Cell Res. 272, 56–61.

Politi, Y., Metzle, R.A., Abrecht, M., Gilbert, B., Wilt, F.H., Sagi, I., Addadi, L., Weiner, S., Gilbert, P.U., 2008. Transformation mechanism of amorphous calcium carbonate into calcite in the sea urchin larval spicule. Proc. Natl Acad. Sci. USA 105, 17362–17366.

Röttinger, E., Saudemont, A., Duboc, V., Besnardeau, L., McClay, D., Lepage, T., 2008. FGF signals guide migration of mesenchymal cells, control skeletal morphogenesis and regulate gastrulation during sea urchin development. Development 135, 353–365.

Smith, A.B., Pisani, D., Mackenzie-Dodds, J.A., Stockley, B., Webster, B.L., Littlewood, D.T., 2006. Testing the molecular clock: molecular and paleontological estimates of divergence times in the Echinoidea (Echinodermata). Mol. Biol. Evol. 10, 1832–1851.

Tekaia, F., Yeramian, E., 2006. Evolution of proteomes: fundamental signatures and global trends in amino acid compositions. BMC Genomics 7, 307.

Thompson, J.D., Higgins, D.G., Gibson, T.J., 1994. CLUSTAL W: improving the sensitivity of progressive multiple sequence alignment through sequence weighting, position-specific gap penalties and weight matrix choice. Nucleic Acids Res. 22, 4673–4680.

Wilt, F.H., Ettensohn, C.A., 2007. Morphogenesis and biomineralization of the sea urchin larval endoskeleton. In: Bauerlein, E. (Ed.), Handbook of Biomineralization. Wiley-VCH, Weinheim, pp. 183–210.

Wilt, F.H., Killian, C.E., Hamilton, P., Croker, L., 2008a. The dynamics of secretion during sea urchin embryonic skeleton formation. Exp. Cell Res. 314, 1744–1752.

Wilt, F., Croker, L., Killian, C.E., McDonald, K., 2008b. Role of LSM34/SpSM50 proteins in endoskeletal spicule formation in sea urchin embryos. Invertebr. Biol. 127, 452–459.

Wu, S.Y., Ferkowicz, M., McClay, D.R., 2007. Ingression of primary mesenchyme cells of the sea urchin embryo: a precisely timed epithelial mesenchymal transition. Birth Defects Res. 81, 241–252.

Zhu, X., Mahairas, G., Illies, M., Cameron, R.A., Davidson, E.H., Ettensohn, C.A., 2001. A large-scale analysis of mRNAs expressed by primary mesenchyme cells of the sea urchin embryo. Development 128, 2615–2627.